9

Analysis of a Supply Chain in Electrical and Electronic Industry

Roberto Ferrauto
Altran Italia S.p.A; Rome, Italy

1. Introduction

This chapter aims to provide a block analysis technique for complex electronic systems. This technique is based on the partitioning of the chain in several functional blocks. Each part of the system is simulated and numerically tested by using the more suitable technique to predict its performance in terms of the analysis of interest. This approach allows an identification of the block responsible for any specification violation and hence a more easy and quick solution of the problem. The simulation techniques can be different and carried out in different domains (time or frequency). The results of each simulation must be then investigated in order to verify if the results are compliant with the passivity and causality check. After the simulation of the complete system is carried out, the parameters of each block are cascaded to get the overall system performances. A flow diagram of the proposed approach is reported in Fig. 1.
This chapter consists in 4 sections. Section 2 describes helpful techniques to predict the frequency content of the input voltage signal. Section 3 describes the different useful ways to numerically characterize the different electronic part. In Section 3.3 the fulfillment of passivity and causality of the port parameters of the results of the simulations is discussed. Section 3.3 describes the evaluation of the DC resistance value of a single block. Finally, in Section 3.4, the computed results can be validated by hardware measurements.

2. Signal spectra

In this section a general overview of the spectral composition of the periodic signals is reported. Pulses described using time are said to be represented in time domain. Most signal integrity work is performed in the time domain, but it's important to understand the way in which the electrical characteristics of the circuit board traces change at different frequencies. The frequency approach is especially useful when studying how losses on transmission lines affect the shape (distortion) and alignment of pulses (intersymbol interference).
Oscilloscope is a common time-domain instrument and the SPICE circuit simulator displays its results in the time domain by default. A vector network analyzer (VNA), which displays the impedance of a component or transmission line at various frequencies, and the spectrum analyzer, a device that simultaneously displays the amplitude across a range of frequencies, is example of frequency-domain instruments.

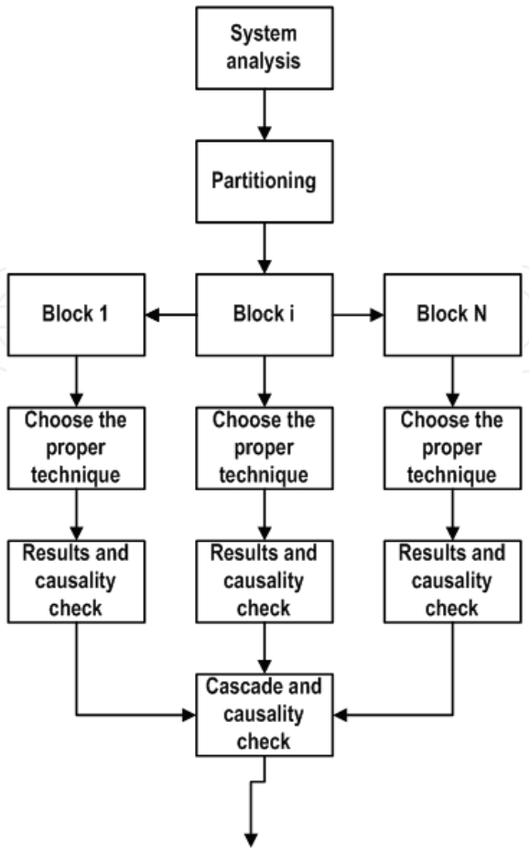

Fig. 1. Flow diagram of the proposed approach

The analysis is concentrated about the signals that are representative of the typical digital products. The waveforms of primary importance in digital circuits are those which represent the clock and the digital data and they are trapezoidal square pulses. These signals are present in the main ICs.
We discuss how time domain factors (rise time, fall time and duty cycle) affect their spectral contents: the spectrum is a function of these parameters.
Taking an infinitive number of harmonics, we could exactly reproduce the signal when we transform back into the time domain. In practice, we don't need to do that; we can show that 15 or 20 harmonics will pretty much guarantee that the signal integrity is preserved. This observation is critical because lossy lines act as low-pass filters and gradually remove higher frequencies. Further, the zero rise time pulses requires more harmonics than an identical pulse having a slower rise time. In the frequency domain this means the zero rise time pulse require more bandwidth than rise time pulses for distortion free transmission. In this section the mathematical model that incorporates the effects of asymmetry between rise and fall edge rates and duty cycle is reported. This model provides bounds of the spectra that will facilitate the analysis of the effects of the signals. Finally some numerical examples are proposed.

2.1 Square pulse spectral analysis

Each square pulse is described by an amplitude A, a pulse width PD τ, a time delay TD and a period T. A rectangular waveform, with parameters A = 1V, TD = 250 ns, PW = 500 ns and P = 1000 ns, is reported in Fig. 2.

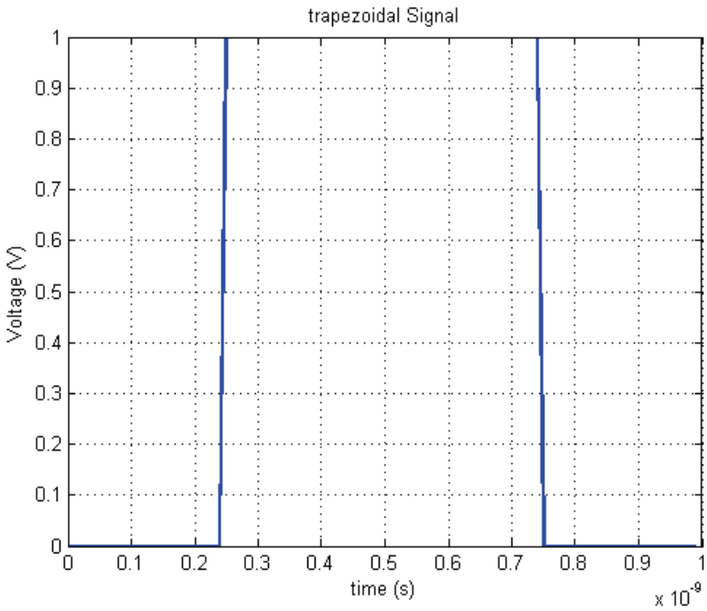

Fig. 2. A = 1 V, TD = 250 ns, T = 1000 ns square pulse

The assessment of the spectral content of this waveform can be carried out using the expansion coefficients of the Fourier series. As a known, a periodic signal x(t), with period T, can be wrote with the series expansion as in (1).

$$x(t) = c_0 + \sum_{n=1}^{\infty} 2|c_n|\cos(n\omega_0 t + \varphi(c_n)) \tag{1}$$

Evaluating the complex-exponential coefficients of the series, c_n, we get the expressions for the amplitude (2) and the phase spectrum (3):

$$|c_n| = \frac{A\tau}{T}\left|\frac{sen(n\pi\tau / T)}{n\pi\tau / T}\right| \tag{2}$$

$$\varphi(c_n) = \pm\frac{n\pi\tau}{T} \tag{3}$$

In Fig. 3 the amplitude spectrum of the square wave we considered as example is reported. The horizontal axes are in terms of cyclic frequency f. The amplitude of the spectral components lie on the envelop that is

$$\frac{A\tau}{T}\left|\frac{sen(\pi f\tau)}{\pi f\tau}\right| \tag{4}$$

This goes to zero where πfτ=mπ or at multiples of $\frac{1}{\tau}$. This function, denoted as $sen(x)/x$, evaluates the unity for x = 0 and is zero for m = 1,2,3,… . Although the continuous envelope bounds the spectral amplitudes, the spectral components only exist at multiples of the fundamental frequency.

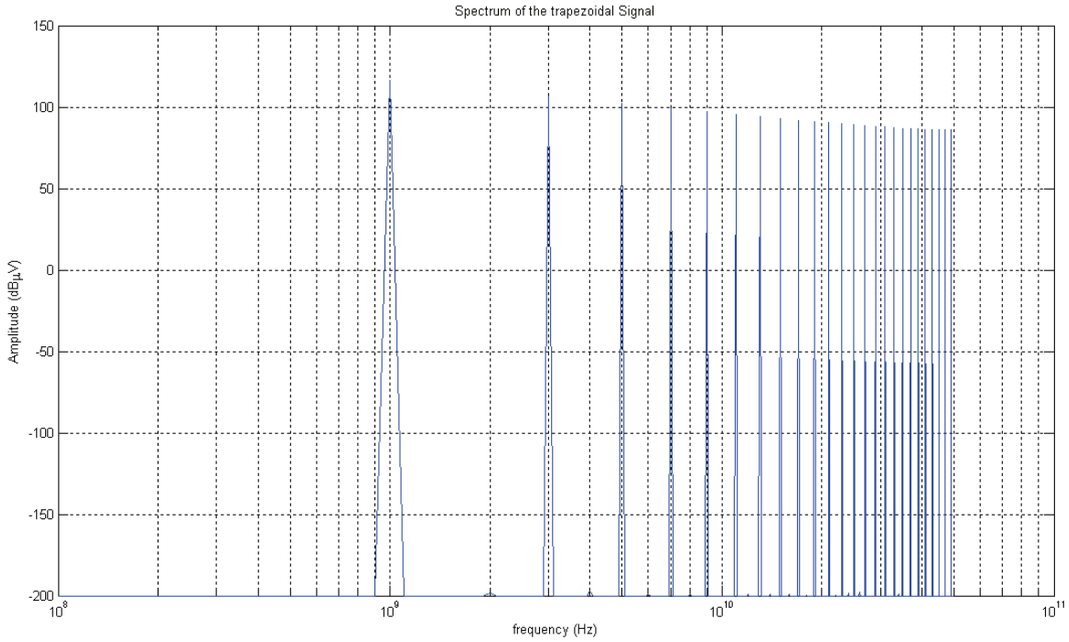

Fig. 3. Amplitude spectrum of the square waveform

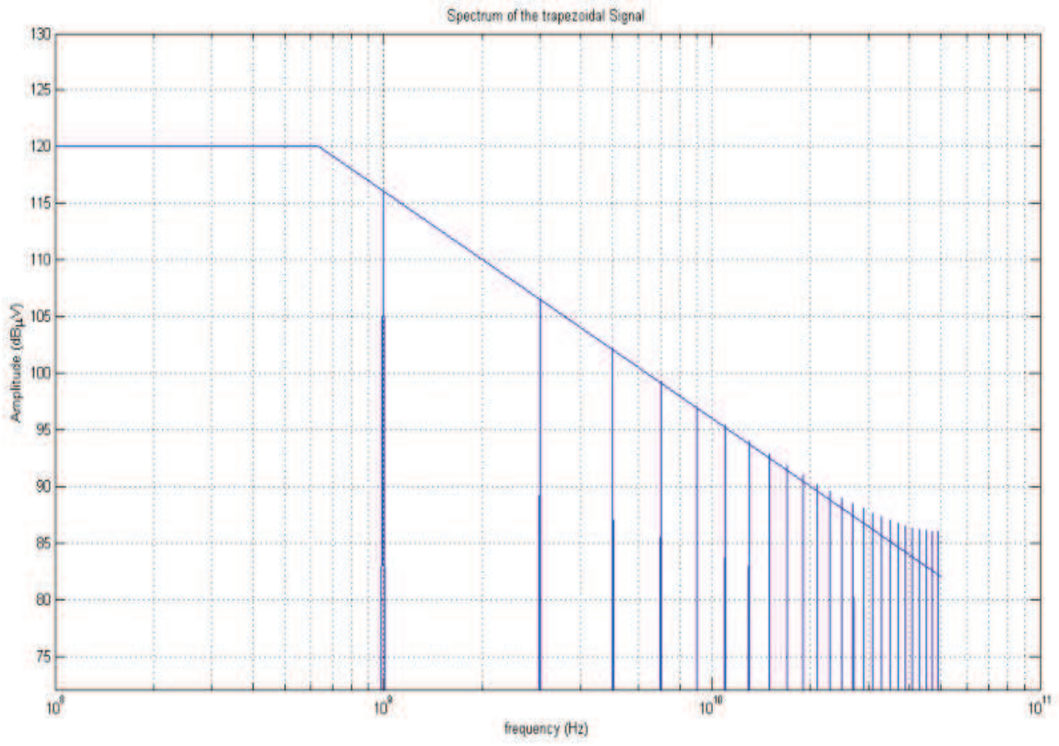

Fig. 4. Bode plot superimposed on FFT of a trapezoidal waveform

Now it's possible to extract more intuitive information from the spectrum expansion coefficients. This allows to generate bounds on the magnitude spectrum. Although these are

upper bounds on the spectral components and are approximate, they are very useful in understanding the impact of pulse width on the spectrum of the waveform. In fact, the spectral components follow a form of $sin(\pi f\tau)/\pi f\tau$. The envelope has zeros at $f = m/\tau$ for m = 1, 2, 3, … . The envelope can be bounded by recalling the small-argument expression for sin *x*, which is that sin $x \cong x$ for x small. This way we get

$$\left|\sin x/x\right| \le \begin{cases} 1 & for\ small\ x \\ 1/|x| & for\ small\ x \end{cases} \tag{5}$$

This can be drawn as two asymptotes, as shown in Fig. 4. The first asymptote is unity and has slope on a logarithmic or Bode plot of 0 dB/decade. The second asymptote decrease linearly of -20dB/decade. The two asymptote converge at x = 1. Thus for the square wave the first asymptote has 0 dB/decade slope out to $f = 1/\pi\tau$ and -20 dB/decade slope above that frequency. Applying this to the reference square wave we get the graph reported in Fig. 4 where to the spectrum is added the upper bound.

2.2 Effect of rise/fall time on spectral content.

We can extend these notions to the trapezoidal pulse train. Each pulse is described by an amplitude A, a pulse rise time τr, a pulse fall time τf, a PD, a PW τ and a period T. A trapezoidal waveform, having A = 1V, T = 1 ns, τr = τf = 0.1 ps, τ = 0.4 ps and PD = 200 ps is reported in Fig. 5.

With the assumption that the rise and fall times are equal, $\tau r = \tau f$, the expansion coefficients expression can be put in the form of the products of two $\sin x/x$ expressions. Replacing the discrete spectrum with a continuous envelope by substituting $f = nT$ we get:

$$\text{envelope} = 2A\frac{\tau}{T}\left|\frac{\sin(\pi\tau f)}{\pi\tau f}\right|\left|\frac{\sin(\pi f\tau_r)}{\pi f\tau_r}\right| \tag{6}$$

In order to produce bounds for this spectrum, we calculate the logarithm of this equation, that produces

$$20\log10(\text{envelope}) = 20\log10(2A\,\tau/T) + 20\log10\left|\frac{\sin(\pi\tau f)}{\pi\tau f}\right| + 20\log10\left|\frac{\sin(\pi\tau_r f)}{\pi\tau_r f}\right| \tag{7}$$

This shows that the composite spectrum is the sum of three pieces:

$$\text{Piece } 1 = 20\log_{10}\left(2A\tau/T\right) \tag{8}$$

$$\text{Piece } 2 = 20\log_{10}\left|\sin(\pi f\tau)/\pi f\tau\right| \tag{9}$$

$$\text{Piece } 3 = 20\log_{10}\left|\sin(\pi f\tau_r)/\pi f\tau_r\right| \tag{10}$$

Piece 1, (8), has 0 dB/decade slope and a constant level of 2Aτ/T=2Aτf0. Piece 2, (9), has two asymptotes. The first asymptote has 0 dB/decade slope. The second asymptote has -20 dB/decade slope. The two asymptotes join at $f = 1/\pi\tau$. Piece 3, (10), consists of two asymptotes, one of which has 0 dB/decade slope and unity level (0 dB) and the other has a -

20 dB/decade slope. The asymptotes of the third piece join at $f = 1/\pi\tau_r$. The composite asymptote thus consists of three straight line segments. The first is due to Piece 1 and has a slope of 0 dB/decade and a starting level of $2A\tau/T$. The second segment has a slope of -20 dB/decade and is due to the Piece 2. The third segment has a slope of -40 dB/decade and is due to the sum of Piece 2 and Piece 3. It is evident that the pulse width must be greater than or equal to the pulse rise/fall times. This way the first breakpoint in the spectral bound will be related to Plot 2, whose breakpoint is related to the pulse width and is $1/\pi\tau$. The second breakpoint is due to Piece 3, whose breakpoint is related to the rise/fall time and is $1/\pi\tau_r$. The spectrum of the waveform showed in Fig. 5 is reported in Fig. 6.

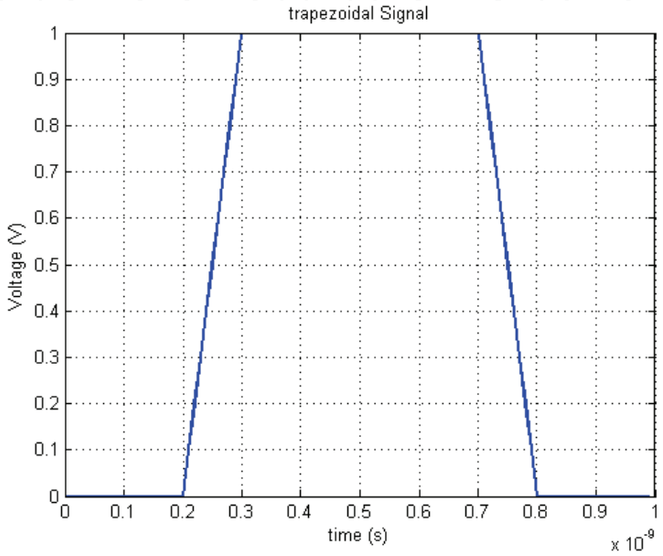

Fig. 5. Trapezoidal square wave

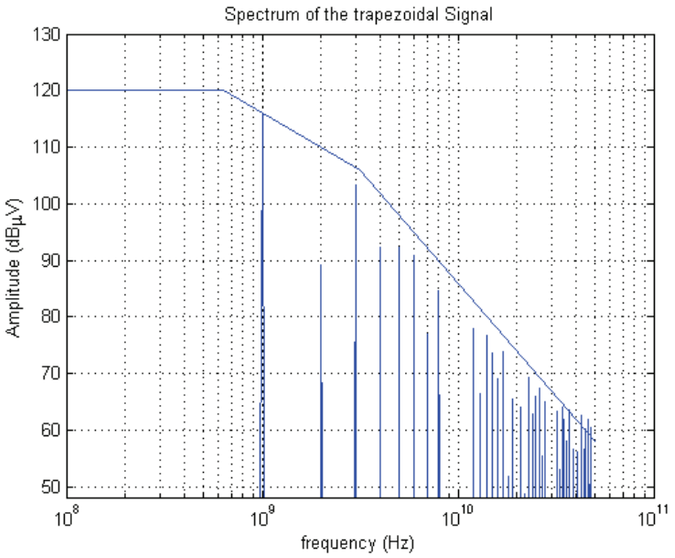

Fig. 6. Spectrum of a trapezoidal waveform having the same rise and fall time

From these spectral bounds it becomes clear that the high-frequency content of a trapezoidal pulse train is primarily due to the rise/fall time of the pulse. Pulses having small rise/fall time will have larger high-frequency spectral content than will pulses having larger rise/fall time. In other words, as rise times increase, the number of significant high order harmonics increase as well. The amplitude of the lower harmonics do not change significantly as rise time increases.

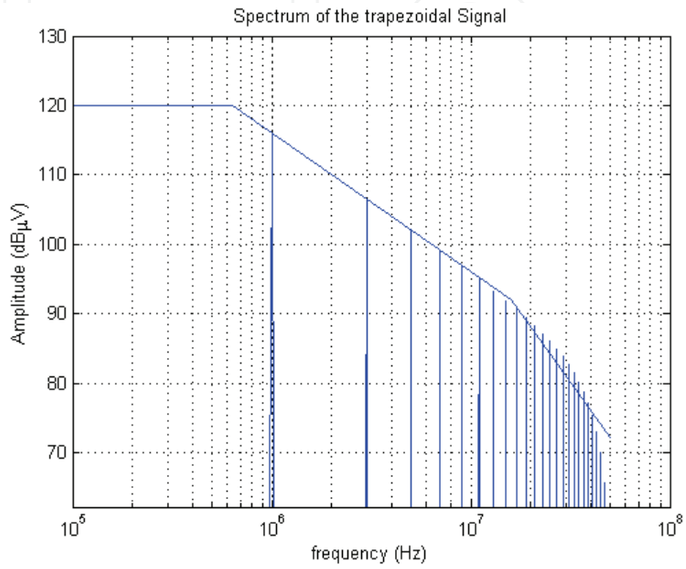

Fig. 7. Spectral bounds for 1 MHz trapezoidal pulse having 20 ns rise/fall time

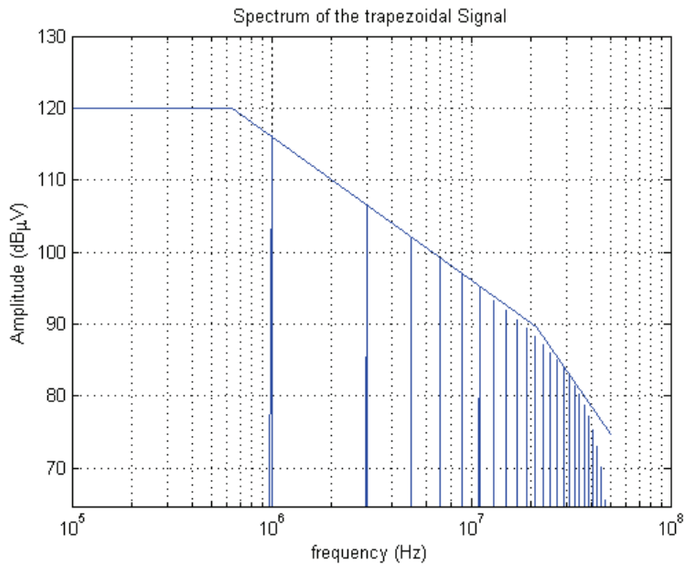

Fig. 8. Spectral bounds for 1 MHz trapezoidal pulse having 15 ns rise/fall time

In order to illustrate this important relationship between pulse rise/fall time and the spectral content of that waveform, we will consider two numerical example.

We will show the spectral bounds for two trapezoidal waveform having:

- A = 1 V, 50% duty cycle, T = 1 μs, $\tau_r = \tau_f$ = 20 ns;
- A = 1 V, 50% duty cycle, T = 1 μs, $\tau_r = \tau_f$ = 15 ns.

The both spectrum are reported in Fig. 7 and Fig. 8.
We can note that the -40 dB/decade bound has moved out from 92 to 89 MHz. The -40 dB/decade breakpoint is commonly used to set the frequency range of analysis where the value of attenuation is enough to neglect the harmonic components at higher frequencies. Anyway, as the spectrogram of a pulse having glitches or plateaus along its edges, or one that overshoots or oscillates about the steady state value, will have more harmonics than the well behaved pulses used here. This leads to take a safe margin of 3-5 times over the -40 dB/decade bandwidth supplied by the numerical analysis.

3. Numerical evaluation

After the frequency range is set, the supply chain, split in several blocks, can be electromagnetically investigated to extract the S-parameters or equivalent circuit. To get a numerically correct response of the chain, the samples of the block are extracted at the same frequency points. Further, a reduction of the interpolation error can be obtained by extracting a large number of samples within the range of analysis. The parameters of each block can be imported in a circuital simulator to get the overall response.
The most important electrical parameters in supply chains analysis are the DC losses and the distortions evaluation of the pulses waveform along the supply chain path.

3.1 Field solver

Electromagnetic field solvers analyze a physical structure such as a circuit board trace or a complex geometry of a connector and produce electrical circuit model. The most common field solvers are those that analyze two dimensional structure (2D solver) while three dimensional structures are analyzed with 3D solvers.

3.1.1 2D field solver

The use of 2D solvers is for those structures having a shape uniform and easily described in only two dimensions. A group of straight circuit board traces that have a constant width, spacing, height above the ground plane, and thickness is a good example of the type of structure appropriate for 2D analysis.
The field solver calculates the resistances, capacitance, inductance, and conductance of the 2D structure and tabulates them across a user defined frequency range. The frequency range must be carefully selected because, as known, digital pulses contain high-frequency harmonics and losses increase with frequency. Since the shape is uniform, the electrical parameters are specified per unit length. The value for a specific trace is found by multiplying the field solver results by the actual length of the structure. The best solver allow the user to choose the output format from a variety of model types, so a library of the circuit models can be created that are usable by a number of different circuit simulators. At the minimum the field solver should produce both an RLGC output file and S-parameters model, preferably in Touchstone files.

3.1.2 3D field solver

Circuit models for physical structures that are not uniform in shape (such as vias or traces that vary in width or spacing or that bend around objects) are created with a 3D field solver.

As the structure is simulated in three dimensions, setting up the problem space is usually more time-consuming and error-prone than with 2D simulators. As in most of the cases the structures consists in multilayer stack-up, the 3D solver have an intuitive graphical interface in order to make easier the check of the circuit board stack-up and defining the material properties and further verify that the values have been assigned properly and assigned to the correct layer in the stack-up.
The drawing interface should be thoroughly tested to determine the ease in creating and editing complex 3D structures. Although some simulators can directly import the 3D mechanical drawings created by CAD drafting software, it's necessary for the designer to "clean up" the drawing and to crop the regions once it has been imported.
Generally the S-parameters are the default output model type.

3.2 Passivity and causality

The EM characterization of the propagating structures is usually determined in frequency domain using equation-based EM solvers or directly by measurements. Anyway, a transformation techniques is required to obtain time-domain transfer function for such passive structures from their frequency domain response. In this process several source of error can be introduced (numerical approximations due to the meshing techniques, finite precision of the computing implementation and the eventually post-processing of the data).
Passivity simply implies that the structure cannot create energy unless there is an energy source, such as a power supply. For example S parameters generated in EM simulators should theoretically be passive. Passivity is the hardest criterion for algorithms to meet and the most difficult physical constraint to satisfy in the current algorithms. Methods that ensure passivity are only practical for small problems. The problem becomes more difficult for multidimensional S-parameters with many ports. For a large number of ports there is no practical way to ensure passivity, and algorithms rely on reasonable checks that work in most cases.
Causality states that the response cannot be obtained before the excitation, so a reflected signal cannot be generated before the incident wave arrives. In other words the signal cannot show up at the load before it leaves the source. This condition is not difficult to meet, but incidentally, it's easy to violate with traditional circuit models.

3.2.1 Passivity check

Reliable time-domain simulation of high-speed simulation systems requires that each part of the system is modeled with sufficient accuracy. In the contrary case, the parameters extracted, when not passive, can lead to an unstable simulations. The stability problem can be avoided by enforcing passivity. To do this several algorithms are available. Passivity enforcement can be implemented on the Y-parameters models and for S-parameters models.
Most of the commercial simulators offer the passive test as standard. This determines if the frequency dependent S-parameters are passive or not.
One of the criterion we can use to carry out the passivity check takes into account the S parameter of the network.
This one calculates the smallest eigenvalue of the matrix $A = I - S^H S$, where I is the identity matrix, S the scattering matrix and the superscript "H" denotes the Hermitian conjugate. For the S matrix to be passive, the smallest eigenvalue of the matrix A defined above should be non-negative. This calculation is performed at each frequency in the sweep. This passivity

criterion is both necessary and sufficient, while the requirement that the magnitude of Sij should not exceed 1 is just necessary.
The result is a real value that is positive or zero at frequencies where the sub-circuit is passive and negative at the frequencies where it is not-passive. This algorithm can be applied to S parameters produced by networks of any number of port. Due to experimental errors and the errors in EM simulations, small eigenvalue result even for passive structures. As example we can consider the computed S parameters of a microstrip filter, whose picture is reported in Fig. 9.

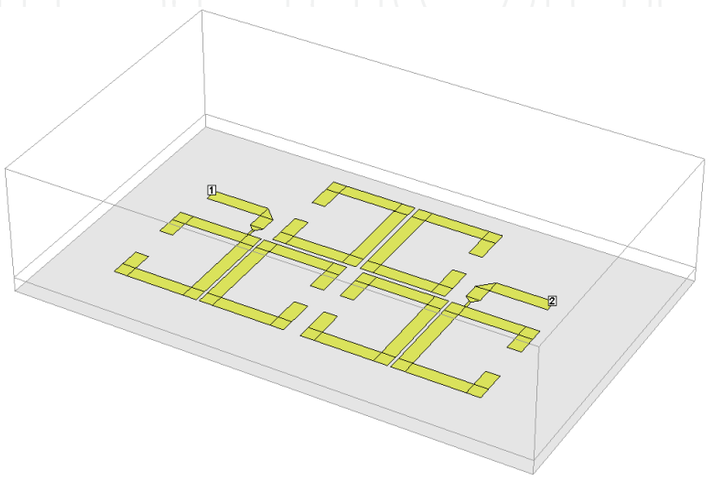

Fig. 9. 11 GHz microstrip filter

The graph of the S parameters is reported in Fig. 10.

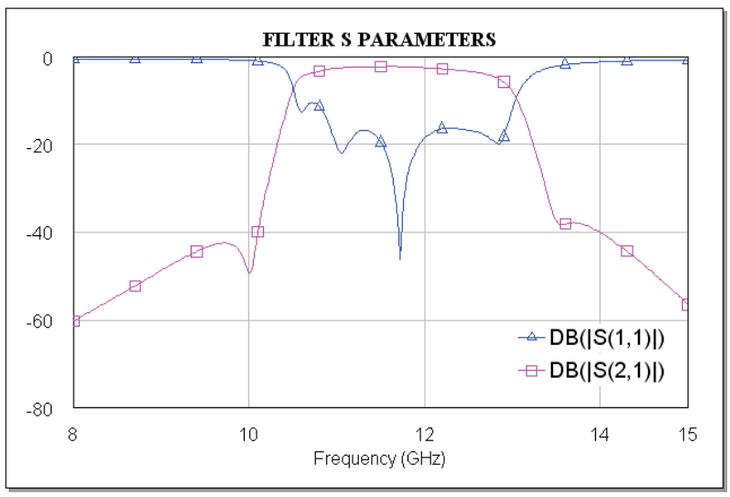

Fig. 10. Achieved 11 GHz microstrip filter S parameters

The result of the passivity check measurement is reported in Fig. 11. This states that the passivity is respected for all the frequency points. Anyway, the passivity can be enforced following the S-parameters calculation. Several iterative algorithms can be implemented to carry out this correction, adding a correction factor, sample by sample.

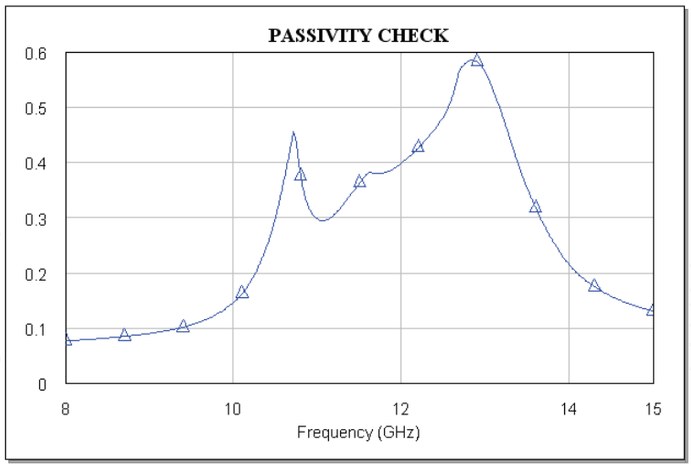

Fig. 11. Graph of 11 GHz filter passivity check result

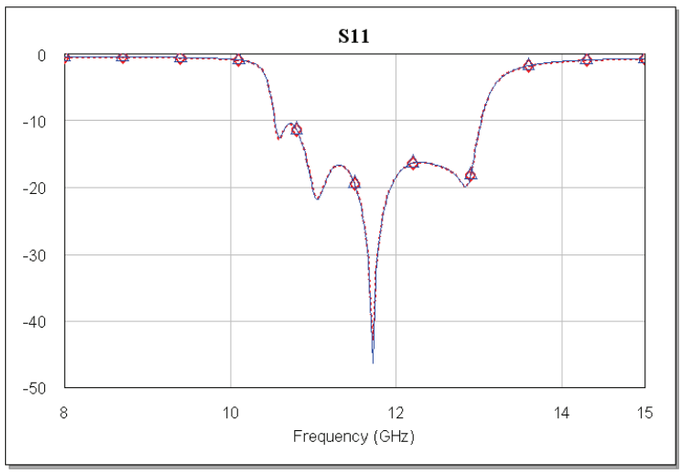

Fig. 12. Computed and passivity enforced S11 curve

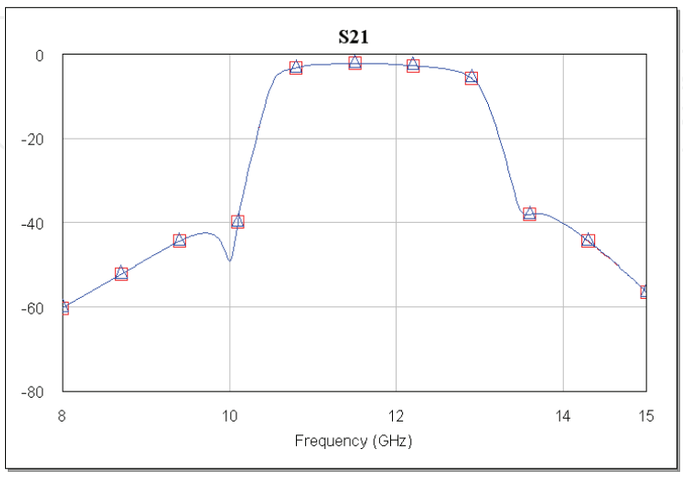

Fig. 13. Computed and passivity enforced S21 curve

Applying the Hamiltonian algorithm to the microstrip filter response, we get the S11 and S21 parameters enforced. In Fig. 12 and Fig. 13 the original and the enforced responses are compared and overlapped. The errors between the two couples of graphs are negligible. In Fig. 14 and Fig. 15 the passivity enforcement errors are reported.

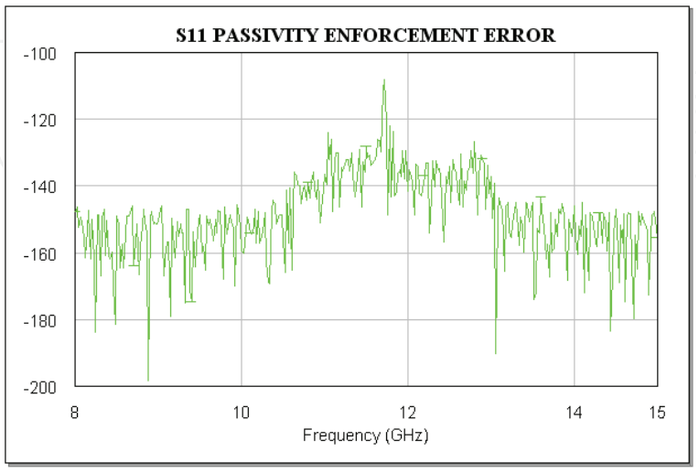

Fig. 14. Error due to the S11 passivity enforcement

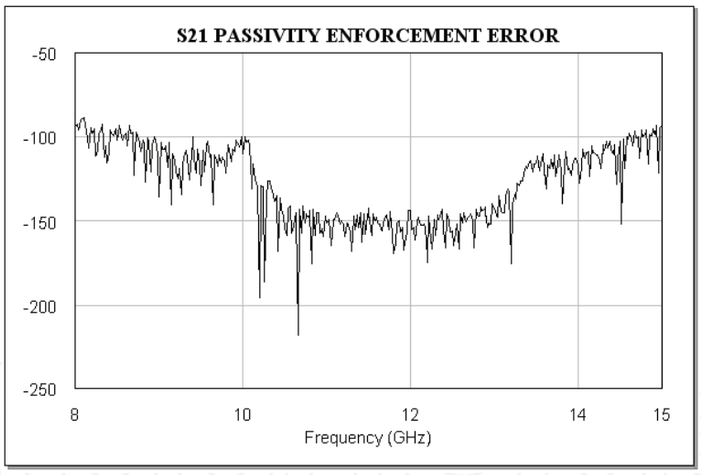

Fig. 15. Error due to the S21 passivity enforcement

3.2.2 Causality check

Before cascading the blocks, each of them must be tested singularly if its multiport frequency dependent characterization matrix (S-parameter, admittance, impedance etc.) fulfils the causality check. In case one or more blocks would not pass this check then they could not be cascaded because their non-causality would render all the system not causal with possible instabilities. The causality check on the extracted S parameters can be performed exciting them with a sinusoidal waveform, within the frequency range of analysis. For each block the physical delay propagation is calculated by evaluating the ratio between the maximum distance and the propagation speed in the block considered.

Comparing the physical delay obtained with that yielded from the simulation, it's possible to conclude if each block is causal or less. We consider a LTCC module, having 1 input port and 3 output ports, Fig. 16.

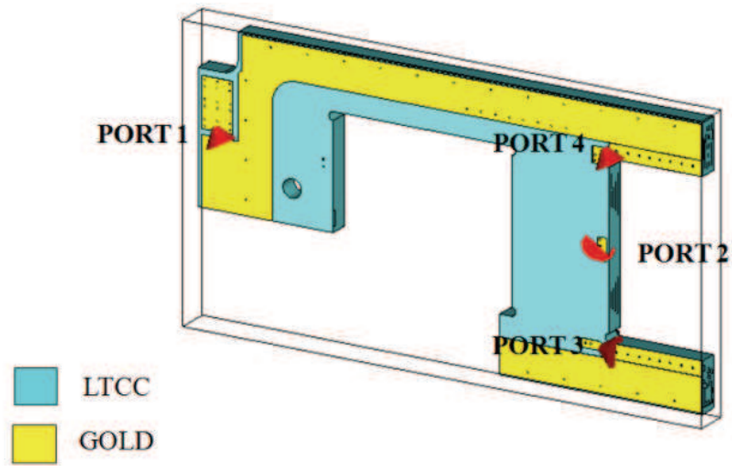

Fig. 16. LTCC module structure

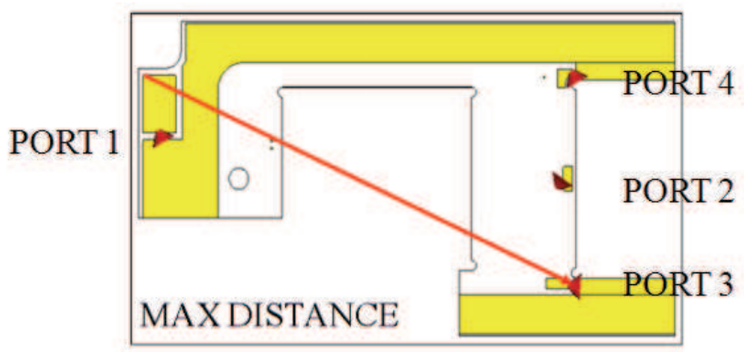

Fig. 17. LTCC module front view with the indication of the maximum distance on the top layer

An EM simulation has been performed to evaluate the S parameters in the range 0-200 MHz. The maximum delay propagation between the input and the output ort is 0.28 ns. Using a circuital simulator, the input port is excited by sinusoidal waveforms in the same range of analysis of the module. If for each frequency, the delay time is higher than the delay time is higher than the delay propagation manually calculated, the model is causal.
In Fig. 18 the schematic of the LTCC model schematic is reported.
In Table 1 the list of the delay propagation manually and schematically evaluated are reported and compared each other. This way we conclude that the LTCC model taken under analysis is causal.
A further test is to import the S parameter of the block under investigation in HSpice schematic. HSpice allows to import only causal models, and if a circuit contains such a model, an error message displays and the circuit is not simulated. If no error is met, it's confirmed that the block also fulfils the causality requirement.

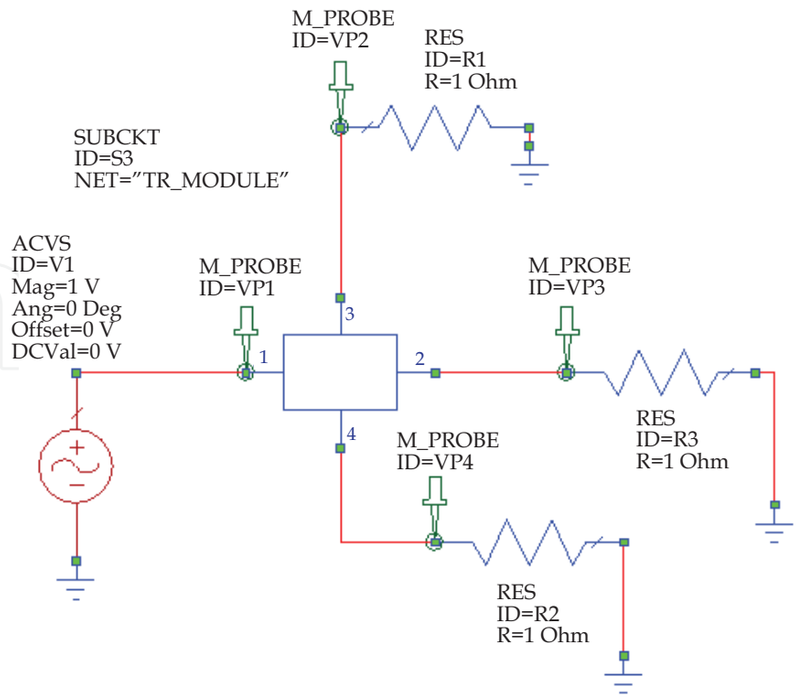

Fig. 18. LTCC module touchstone file in AWR MWO environment

	PHYSICAL DELAY TIME (ns)	DELAY TIME DETECTED VPROBE1 (ns)	DELAY TIME DETECTED VPROBE2 (ns)	DELAY TIME DETECTED VPROBE3 (ns)
@1 MHz	0.28	4.682	4.269	4.153
@5 MHz	0.28	4.598	4.196	4.062
@10 MHz	0.28	4.416	4.021	3.895
@50 MHz	0.28	2.983	2.665	2.563
@100 MHz	0.28	2.043	1.794	1.725
@150 MHz	0.28	1.533	1.345	1.299
@200 MHz	0.28	1.222	1.081	1.050

Table 1. List of the propagation delays manually evaluated compared with the ones evaluated in the schematic

3.2.3 Analytical causality enforcement

The Hilbert transform is used as tool to assess the consistency of measured or numerically computed network transfer functions with respect the causality conditions.

The application of the inverse Fourier integral to the complete frequency response of any physical network should always yield a causal time-domain impulse response. In practice, however, the frequency response information we have is often incomplete (band limited and on a discrete and frequency point grid) and can contain measurements errors. A native application of inverse Fourier integral to such a frequency response almost always yields an incorrect non-causal time-domain model. The Kramers-Kronig relation is very useful in

these situation because it allows us to correct the frequency response and built a causal time-domain model.

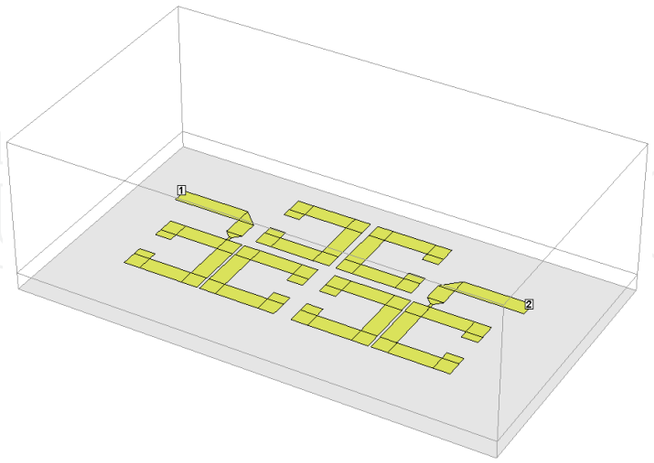

Fig. 19. 20 GHz microstrip filter

Further, these relations give a condition that is both necessary and sufficient, so even before applying an inverse Fourier integral, we can determine whatever a given frequency response will yield a causal or non-causal impulse response. If the real and imaginary part are Hilbert transform of each other, the pulse response is causal, and not otherwise. This fact is very useful because it allows us to test whatever or not a frequency response is causal without ever having to leave the frequency domain.
We apply the causality enforcement to the S parameters of the microstrip filter of Fig. 19. In Fig. 20 and Fig. 21 the computed, red trace, and causality enforced, blue trace, S11 and S21 parameters in the range of analysis are reported.
In both some violation at the borders of the frequency spectrum appear. They are due to the approximation of the numerically computed Hilbert Transform. In Fig. 22 and Fig. 23 the errors produced by the causality enforcements are reported. The levels of causality violations are negligible in the band of operation of the filter.

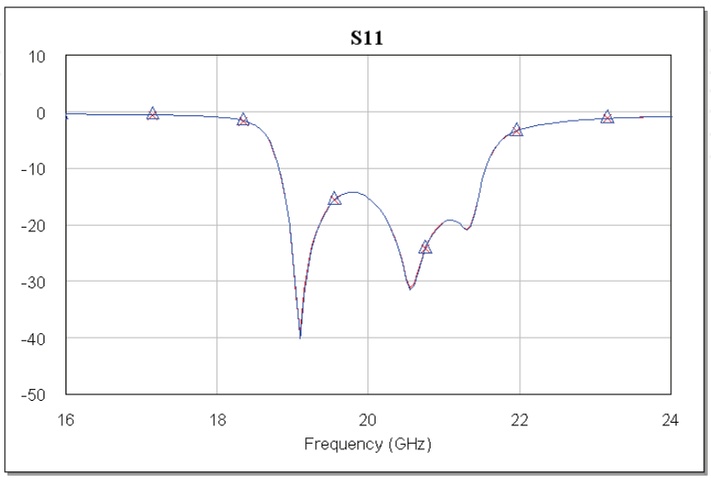

Fig. 20. Computed and causality enforced S11 parameter

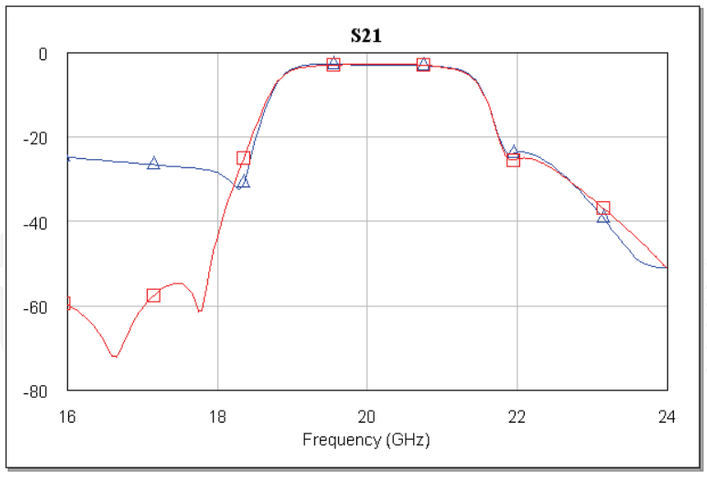

Fig. 21. Computed and causality enforced S21 parameter

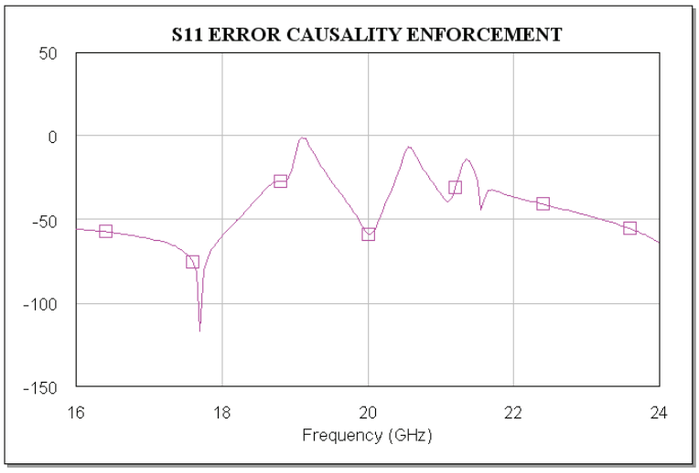

Fig. 22. Error due to the S11 causality enforcement

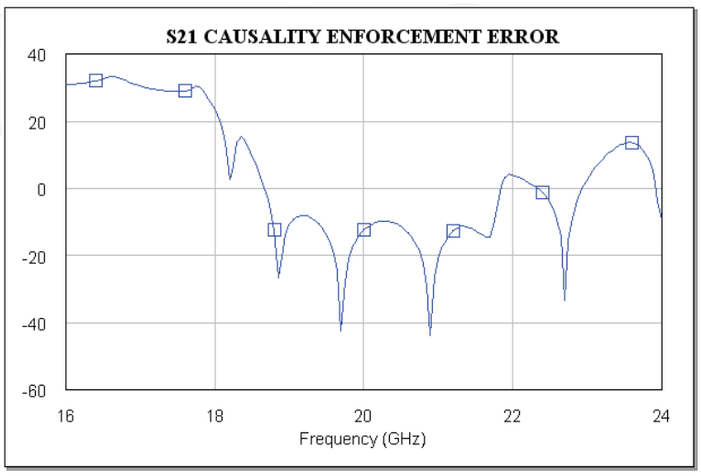

Fig. 23. Error due to the S21 causality enforcement

3.3 DC performance analysis

The last step in this systematic analysis is the evaluation of the DC voltage drop (also known as IR-drop) across each block between their input and output ports. The IR-drop is generally defined as the dc voltage drop across a conductive element due to the dc current flow. The power supply chain in single or multi-layer structure, from the voltage regulator module to the supplied integrated circuits, is affected by the IR drop across each single block planes.
As example we can compute the spatial distribution of the DC electric potential on the conductive parts of a PCB multilayer structure, when a known DC current is injected at their ports.

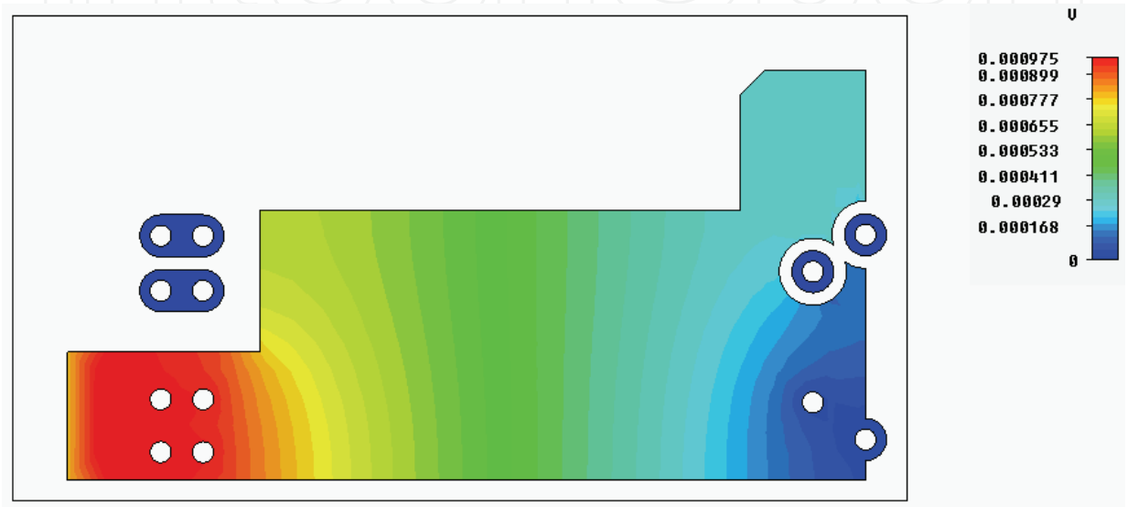

Fig. 24. Spatial distribution of the DC electric potential along the power PCB layer

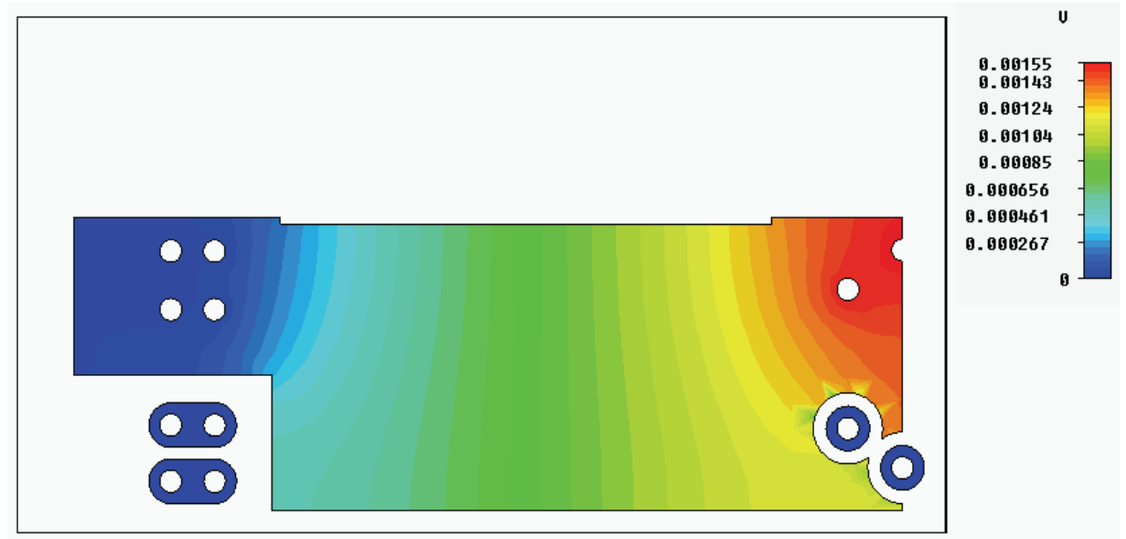

Fig. 25. Spatial distribution of the DC electric potential along the ground PCB plane

For this analysis, due to the complex shapes of the conduction paths, a three dimensional static solver for the current density is used. After having set the ports where the DC current

is injected and drawn, the spatial distribution of the static electric potential between the ports pair is computed. Fig. 24 and Fig. 25 show the voltage distribution for both power and ground layers. From this information it is possible to extract the overall equivalent DC resistance, 2.525 mΩ.
After the DC voltage drop for each block is computed, adding them, the equivalent supply chain DC resistance is known.

3.4 Computed results and measurement validation

All the blocks can be cascaded in order to compute the overall system response. The blocks are imported in a circuital simulator that, using a convolution procedure allows to mix, in the same run, blocks characterized in time domain (as the input voltage source) and blocks characterized in frequency domain.
The voltage pulse is injected at the input port and is evaluated the attenuation and the distortion corresponding at all the output ports. In Fig. 26 the schematic of a supply chain in a circuital simulator environment is reconstructed.

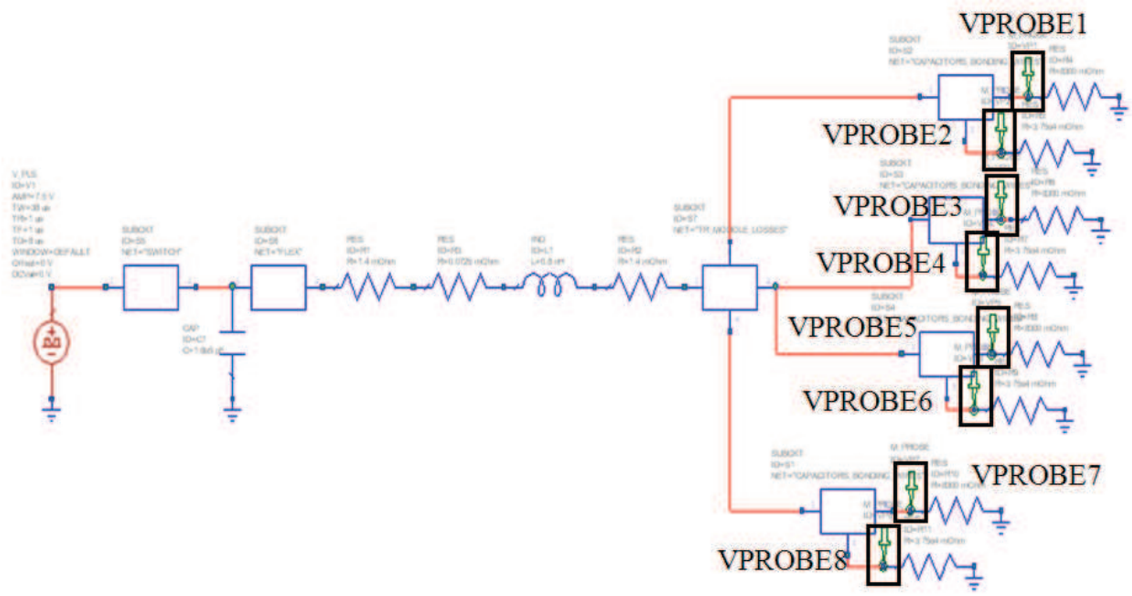

Fig. 26. Schematic of a supply chain

The computed output signals are detected at each output port. In order to validate the developed equivalent model of the supply chain some voltage measurement have to perform on selected nodes and compared with the simulation results. The signals measured at the test points can be compared with the computed ones and the two ones can be overlapped to check the reliability of the proposed approach, Fig. 27 and Fig. 28.

4. Conclusions

This chapter describes a systematic approach for the analysis of the signal integrity of a supply voltage pulse propagating from the input to the output port of a complex supply chain of a devices for spatial and military applications. The use of different approaches and different standard tools makes possible to predict the voltage level and the transient

waveform of the propagating pulse in each section of the complex signal path. The instruments to validate the computed and measured parameters are discussed. To validate this analysis approach the measure on the real device has to be performed.

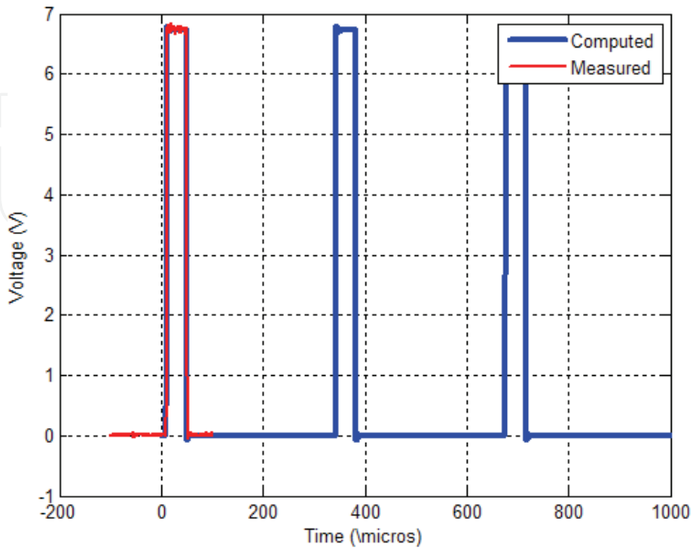

Fig. 27. Comparison between computed and measured transient voltage waveform

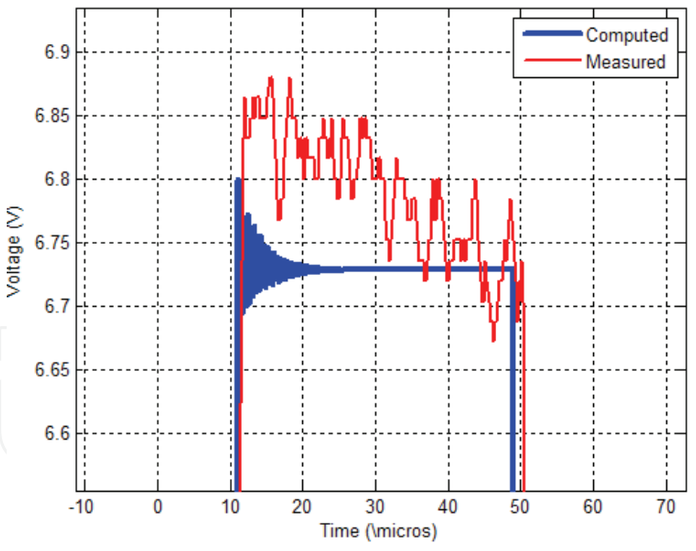

Fig. 28. Comparison between the computed and measured waveform

5. References

A. C. Cangellaris, M. Celik, S. Pasha,, L. Zhao, "Electromagnetic model order reduction for system level modeling, IEEE Trans. Microwave Theory Techn., vol. 47, n. 6, June 1999, pp. 840-850.

Agilent Technologies, Advanced Design Simulator, www.agilent.com, 2010.
AWR, Microwave Office 2009, www.awr.com, 2009.
B. Archambeault, C. Brench, O. Ramahi, EMC/EMI Computational Modeling Handbook, II Edition, Kluwer Academic Publishers, 2001.
C. R. Paul, Introduction to Electromagnetic Compatibility, II Edition, Wiley InterScience Publication, New York, USA, 2009.
Computer Simulation Technology, CST Studio 2010, www.cst.com, 2010.
F. M. Tesche, "On the use of Hilbert transform for processing measured CW data", IEEE Transactions on Electromagn. Compatibility, vol. 34, n. 3, August 1992, pp. 259-266.
G. Antonini, A. Ciccomancini Scogna, A. Orlandi, "De-Embedding procedure based on computed/measured data set for PCB structure characterization", IEEE Trans. on Advanced Packaging, vol. 27, n. 4, Nov. 2004, pp. 597-602.
G.Antonini, A.Orlandi, V.Ricchiuti,"Causality Check for SI Data Validation", in Proc. of 9th IEEE Workshop on Signal Propagation on Interconnects, Garmish-Partenkirchen, Germany, May, 2005.
Hsien-Te Chen; Chieh-Chun Chang; TingTing Hwang, "New spare cell design for IR drop minimization in Engineering Change Order", in Proc. of 46th Design Automation Conference, San Francisco, CA, USA, 26-31 July 2009 pp. 402 – 407.
H. W. Bode, Network Analysis and Feedback Amplifier Design, Van Nostrand, NJ, USA, 1945.
K. M. Coperich Branch, J. Morsey, A. C. Cangellaris, A. E. Ruehli, "Physically consistent transmission line models for high-speed interconnects in lossy dielectrics", IEEE Trans. Adv. Packag., vol. 25, n. 2, May 2002, pp.129-135.
R. Ferrauto, F. De Paulis, E. Ippoliti, F. Vasarelli, A. Orlandi, "IR-Drop Simulation using CST STUDIO SUITE", CST Application Note nr. 71, March 2009.
Robert S. Elliot, Waves and Microwave Circuits, Prentice Hall International, Inc, 1993.
S. L. Hahn, Hilbert Transform in Signal Processing, Artech House Publishers, 2000.
Sonnet Software, Sonnet EM simulator, www.sonnetsoftware.com, 2010.
Synopsis, HSpice, http://www.synopsys.com/Tools/
T. Weiland, "A Discretization Method for the Solution of Maxwell's Equation for Six Component Fields", Electronics and Communication, (AEÜ), Vol.31 (1977), p. 116.

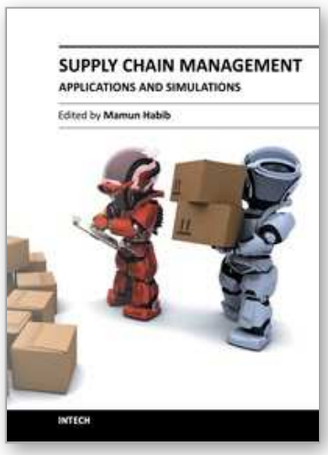

Supply Chain Management - Applications and Simulations
Edited by Prof. Dr. Md. Mamun Habib

ISBN 978-953-307-250-0
Hard cover, 252 pages
Publisher InTech
Published online 12, September, 2011
Published in print edition September, 2011

Supply Chain Management (SCM) has been widely researched in numerous application domains during the last decade. Despite the popularity of SCM research and applications, considerable confusion remains as to its meaning. There are several attempts made by researchers and practitioners to appropriately define SCM. Amidst fierce competition in all industries, SCM has gradually been embraced as a proven managerial approach to achieving sustainable profits and growth. This book "Supply Chain Management - Applications and Simulations" is comprised of twelve chapters and has been divided into four sections. Section I contains the introductory chapter that represents theory and evolution of Supply Chain Management. This chapter highlights chronological prospective of SCM in terms of time frame in different areas of manufacturing and service industries. Section II comprised five chapters those are related to strategic and tactical issues in SCM. Section III encompasses four chapters that are relevant to project and technology issues in Supply Chain. Section IV consists of two chapters which are pertinent to risk managements in supply chain.

How to reference
In order to correctly reference this scholarly work, feel free to copy and paste the following:

Roberto Ferrauto (2011). Analysis of a Supply Chain in Electrical and Electronic Industry, Supply Chain Management - Applications and Simulations, Prof. Dr. Md. Mamun Habib (Ed.), ISBN: 978-953-307-250-0, InTech, Available from: http://www.intechopen.com/books/supply-chain-management-applications-and-simulations/analysis-of-a-supply-chain-in-electrical-and-electronic-industry

INTECH
open science | open minds

InTech Europe
University Campus STeP Ri
Slavka Krautzeka 83/A
51000 Rijeka, Croatia
Phone: +385 (51) 770 447
Fax: +385 (51) 686 166
www.intechopen.com

InTech China
Unit 405, Office Block, Hotel Equatorial Shanghai
No.65, Yan An Road (West), Shanghai, 200040, China
中国上海市延安西路65号上海国际贵都大饭店办公楼405单元
Phone: +86-21-62489820
Fax: +86-21-62489821

IntechOpen